IIETA International Information and Engineering Technology Association
Advancing the World of Information and Engineering

Annales de Chimie - Science des Matériaux
Vol. 50, No. 1, February, 2026, pp. 23-31
Journal homepage: http://iieta.org/journals/acsm

Microstructure-Controlled Fatigue Crack Initiation and Early Growth in Super Duplex Stainless Steel 2507

Jaber Ali Zghair[1], Mustafa Abdulhussein Lafta[2], Ameer Abid Muslim[2], Laith Ali Zgair[1], Haider Fawzi Mahmood[1*]

[1] Department of Machines and Equipment Engineering Technologies, Al-Mussaib Technical College, Al-Furat Al-Awsat Technical University, Kufa 51009, Iraq
[2] Department of Water Resources Technology, Al-Mussaib Technical Institute, Al-Furat Al-Awsat Technical University, Kufa 51009, Iraq

Corresponding Author Email: haider.fawzi@atu.edu.iq

https://doi.org/10.18280/acsm.500103

Received: 28 November 2025
Revised: 5 February 2026
Accepted: 15 February 2026
Available online: 28 February 2026

Keywords:
duplex stainless steel 2507, fatigue crack initiation, microstructure-property relationship, phase boundaries, Electron Backscatter Diffraction, Digital Image Correlation

ABSTRACT

The present study proposes a method to detect fatigue crack initiation and propagation in super duplex stainless steel 2507, particularly based on microstructural and crystallographic characteristics. Microstructure-fatigue property correlation has also been assessed using Scanning Electron Microscopy (SEM), Electron Backscatter Diffraction (EBSD), Digital Image Correlation (DIC), and in-situ fatigue tests. Over 250 fatigue crack initiation sites have been evaluated, and the results show that 78% of the fatigue crack initiations occur at austenite-ferrite phase boundaries, where the stress/strain concentration is higher compared to grain boundaries. Phase-dependent fatigue crack propagation indicates that the austenite phase crack propagation rate is 34% lower than ferrite phase crack propagation rates for cracks less than 25 μm. Fatigue crack propagation across the grain boundaries depends significantly on the misorientation between the grains. The fatigue crack propagation across the grain boundaries decreases from 85% for low-angle grain boundaries to less than 20% for high-angle grain boundaries. The DIC mapping also shows strain localization at the phase boundaries and triple points, which are the fatigue crack initiation locations. The Weibull analysis has shown that the shape parameter is approximately 3.2, which indicates a consistent fatigue response for cyclic loading conditions. It has also been observed that the microstructural features play a major role in fatigue crack initiation for duplex stainless steel 2507.

1. INTRODUCTION

Super duplex stainless steels (SDSSs) have found increased preference as fatigue-critical component materials in the offshore industry, marine industry, and chemical processing industry owing to superior mechanical and corrosion properties in hostile environments and fatigue loading conditions [1]. Among the family of SDSSs, UNS S32750 (SDSS 2507) finds extensive application in structural components of mechanical systems in which fatigue crack initiation and propagation play major roles in determining the service life of the components [2].

The unique two-phase microstructure of duplex stainless steels with nearly equivalent volume fractions of austenite and ferrite exhibits inherent mechanical heterogeneity at the microscale [3]. During fatigue loading conditions, the incompatibility in elasticity and plasticity of the two phases of the material will cause stress and strain concentration in the material, greatly influencing fatigue crack initiation and propagation of short cracks.

Previous studies have revealed that fatigue crack initiation in metallic alloys is greatly influenced by the inherent heterogeneity of the material at the microscopic scale, including grain boundaries, phase interfaces, and orientation relationships [4, 5]. In the case of duplex stainless steels, the austenite-ferrite phase boundary has been identified as a major site of fatigue crack nucleation in the material owing to the incompatibility of the elastic modulus of the two phases of the material [6, 7].

In spite of extensive research, quantitative understanding of fatigue crack initiation, as well as early crack growth, in super duplex grades is still in its infancy. Most of the research has been focused on macroscopic fatigue life, with less emphasis on short crack growth, which is more sensitive to microstructural effects [8]. In fact, recent research has shown that environmental effects such as seawater exposure, cathodic protection, as well as hydrogen uptake, can further accentuate microstructure-controlled fatigue in SDSSs, highlighting the need for a more detailed understanding of fatigue crack initiation/early growth mechanisms in duplex stainless steels [9, 10].

In recent years, advances in experimental characterization techniques, such as Electron Backscatter Diffraction (EBSD), Digital Image Correlation (DIC), and in-situ fatigue testing,

now open up new avenues for investigating fatigue crack initiation/early growth in duplex stainless steels [11]. Electron backscattered diffraction can be used for a detailed characterization of crystallographic texture, grain misorientations, as well as deformation accumulation in duplex stainless steels [12]. DIC can be used for a direct measurement of strain localization, as well as plastic zone formation in duplex stainless steels, during cyclic fatigue loading. In fact, a combination of in-situ fatigue testing, electron backscattered diffraction, DIC, as well as high-resolution SEM fractography can now be used for a comprehensive investigation of fatigue crack initiation/early growth in duplex stainless steels [13, 14].

In this context, the present research aims at presenting a comprehensive experimental investigation of fatigue crack initiation/early growth in super duplex stainless steel 2507 using SEM, EBSD, DIC, as well as in-situ fatigue testing, complemented by statistical analysis. The specific research aims include: (i) identifying major microstructural crack initiation sites in duplex stainless steels, (ii) quantifying early crack growth in duplex stainless steels, (iii) investigating crystallographic misorientations in duplex stainless steels, as well as (iv) establishing quantitative microstructure-fatigue relationships in duplex stainless steels, which can be used for design/development of advanced duplex stainless steels.

Unlike previous studies that focus mainly on macroscopic fatigue life of duplex stainless steels, this work provides a quantitative microstructure-controlled analysis of fatigue crack initiation and early crack propagation in SDSS 2507 using an integrated SEM–EBSD–DIC–in-situ fatigue framework. The study establishes statistical relationships between phase boundaries, crystallographic misorientation, and crack propagation kinetics, which provide new insights for microstructure-based fatigue design of duplex stainless steels.

2. MATERIALS AND EXPERIMENTAL METHODS

2.1 Material selection and processing

The material that is being examined in the present study is a commercially available super duplex stainless steel, UNS S32750, also known as 2507. The reason why this specific material has been selected for the present study is that it is being extensively used in industries that are known for being highly fatigue-prone. The material was machined into specimens of 50 mm length to facilitate fatigue testing and microstructural characterization. The chemical composition and microstructure were verified by a manufacturer who had subjected the material to solution annealing at 1080 °C for 30 minutes, followed by water quenching, to produce the optimum two-phase microstructure.

The heat treatment ensured that all undesirable intermetallic were dissolved, and at the same time, it ensured that a stable microstructure was achieved with nearly balanced amounts of austenite and ferrite. The chemical composition was also verified through optical emission spectroscopy (OES), which was carried out according to standard procedures, and it was confirmed that it complies with the chemical as per the applicable material specification standards. The results also confirmed that chromium, nickel, molybdenum, and nitrogen were at desired levels, which is important for super duplex stainless steels of high performance.

The chemical composition of the investigated UNS S32750, carried out through OES, which was carried out according to standard procedures. The chemical composition is shown in Table 1 and is consistent with the nominal composition of UNS S32750, and as a result, it is ensured that a stable microstructure is achieved.

Table 1. Chemical composition of super duplex stainless steel 2507 (wt.%)

Element	Cr	Ni	Mo	Mn	Si	N	C	Fe
wt.%	25.1	7.0	4.0	1.2	0.6	0.27	0.02	Bal.

2.2 Advanced microstructural characterization

2.2.1 Sample preparation for multi-scale analysis

The specimens for microstructural characterization were prepared with special attention paid to avoiding surface damage and deformation, especially for materials that were to be prepared for high-resolution analysis. The procedures adopted were:

- Low speed diamond cutting, which minimized any deformation
- Sequential grinding with SiC papers up to 4000 grit
- Polishing with 6 µm and 1 µm suspensions of diamond powder

This microstructural preparation method for EBSD analysis is an optimized method, and strain-free surfaces with minimal topological relief between the austenite and ferrite microconstituents have been achieved.

2.2.2 Phase identification and quantitative analysis

Microstructural analysis of the alloy has been conducted using a variety of microstructural analysis techniques to ensure the accuracy of phase identification and quantitative analysis.

- Optical Microscopy

Initial microstructural analysis of the alloy has been conducted using a Zeiss Axioplan 2 optical microscope after etching the microstructure using Beraha's etchant (100 ml H2O + 20 ml HCl + 0.3 g K2S2O5).

- Quantitative Metallography

Phase volume fractions, grain size distribution, and morphological characteristics have been conducted according to ASTM E562 using a systematic point counting technique with a minimum of 1000 points per sample [15].

- Scanning Electron Microscopy (SEM)

High-resolution microstructural analysis has been conducted using a JEOL JSM-7001F field emission SEM operating at accelerating voltages of 15-20 kV.

2.2.3 Electron Backscatter Diffraction analysis

EBSD analysis has been conducted to obtain microstructural data related to the fatigue crack initiation and propagation mechanisms. EBSD analysis has been conducted using an Oxford Instruments AZtec EBSD system coupled with a JEOL JSM-7001F FESEM [16].

- EBSD Analysis Parameters
- Accelerating Voltage: 20 kV
- Working Distance: 15 mm
- Probe Current: 1.5 nA
- Step Size: 0.2 µm (0.1 µm in high-resolution regions)
- Pattern Resolution: 1344 × 1024 pixels
- Indexing Rate: > 95%

2.3 Fatigue testing program

2.3.1 Standard fatigue testing

Fatigue tests were conducted with the aid of an MTS 810 servo-hydraulic testing machine under load control conditions. Dog-bone-shaped samples were machined according to ASTM E466 standards with a gauge length of 25 mm and gauge diameter of 6 mm. Meanwhile, surface roughness maintained Ra < 0.4 µm and stress concentration factor Kt < 1.05.

Testing conditions used sinusoidal loading with stress ratio R = 0.1 at 20 Hz frequency. All tests were performed in air at 23 ± 2 ℃ with stress range from 280 MPa to 500 MPa.

2.3.2 Interrupted fatigue testing

Interrupted fatigue tests were conducted in order to evaluate the crack initiation and early stages of crack propagation in the material under investigation. Interrupted tests were conducted at specified fractions of fatigue life (N/Nf = 0.1, 0.3, 0.5, 0.7, and 0.9). Interrupted tests were followed by surface analysis of the samples with the aid of SEM to identify locations of crack initiation and growth.

2.3.3 In-situ fatigue testing

Fatigue tests were conducted with the aim of understanding the process of crack nucleation and growth in the material under investigation with the aid of a Kammrath & Weiss micro-fatigue stage in the SEM chamber.

Miniature samples of size 15 mm × 3 mm × 1 mm with single-edge notch were used in the tests.

Tests were conducted under load control with stress ratio R = 0.1 and frequency of 0.1 Hz.

High-resolution images and videos were taken periodically throughout the tests.

2.4 Fatigue crack growth modeling

To interpret the experimentally observed fatigue crack growth, the fatigue crack growth rate was calculated using the classical Paris–Erdogan equation. The equation correlates the fatigue crack growth rate with the stress intensity factor range under cyclic loading conditions.

Crack growth rate:

$$\frac{da}{dN} = C(\Delta K)^m \quad (1)$$

where, da/dN represents the fatigue crack growth rate, whereas C and m are the constants for the specific material under consideration, and ΔK represents the stress intensity factor range.

For a surface crack, the stress intensity factor range can be related as:

$$\Delta K = Y\sigma\sqrt{\pi a} \quad (2)$$

where, Y represents the correction factor, σ represents the stress, and a represents the length of the crack. The aforementioned equations delineate the theoretical basis for comprehending the empirically observed fatigue fracture propagation rate in duplex stainless steel 2507.

2.5 Digital Image Correlation analysis

2.5.1 Digital Image Correlation system configuration

The local strain field surrounding the microstructural features and cracks was obtained by utilizing a high-resolution stereo DIC system with dual 5-megapixel CCD cameras and telecentric lenses for accurate sub-pixel measurement. The Vic-3D commercial software was utilized for image correlation and post-processing.

2.5.2 Digital Image Correlation measurement protocol

The optimized speckle pattern was used by employing a white titanium dioxide base coat with a black activated carbon speckle pattern, which gave a speckle size of 3 to 5 pixels and a surface coverage of 50 to 60%.

The parameters used for the measurement were a subset size of 25 × 25 pixels, a step size of 5 pixels, a strain resolution of 50 µstrain, and a displacement resolution of 0.01 pixels. Regular calibration was performed to ensure precise measurement.

2.6 Statistical analysis and data processing

2.6.1 Crack initiation statistics

The crack initiation behavior was statistically analyzed by making use of a database with a minimum of 50 crack initiation points per test condition. Crack initiation points were grouped based on the crack initiation point location with respect to the microstructure, crystallographic orientation, stress concentration, and proximity to the microstructure.

2.6.2 Electron Backscatter Diffraction data processing

The EBSD data processing was performed by making use of the Oxford AZtec software as well as the MTEX MATLAB toolbox to perform noise reduction, grain reconstruction with a threshold of 5°, grain boundary energy estimation by making use of the Read-Shockley model, Taylor factor estimation, and geometrically necessary dislocation density estimation.

2.7 Fractographic analysis

2.7.1 Fracture surface preparation

The fracture surfaces were cleaned thoroughly using ultrasonic baths containing acetone and ethanol, each for a period of 10 minutes. Subsequently, the fracture surfaces were dried using warm air, after which they were stored in a desiccated environment.

2.7.2 Multi-scale fractographic examination

The fracture surfaces were examined at low magnification using stereomicroscopy, which helped to analyze the crack initiation sites, crack growth, as well as the fracture sites. High-resolution SEM examination was carried out to investigate crack initiation, fatigue striations, spacing between striations, secondary crack networks, and phase-dependent fracture mechanisms.

The research methodology adopted in the current research is suitable for the systematic investigation of the effects of microstructures on fatigue crack nucleation and early stages of crack growth. The combination of techniques, i.e., EBSD, DIC, in-situ fatigue testing, and statistical analysis, provides a solid foundation for the development of a microstructure-based fatigue life prediction model, especially for super duplex stainless steels.

The overall experimental workflow adopted in this study, including microstructural characterization, fatigue testing, DIC strain analysis, and statistical crack evaluation, is summarized in Figure 1.

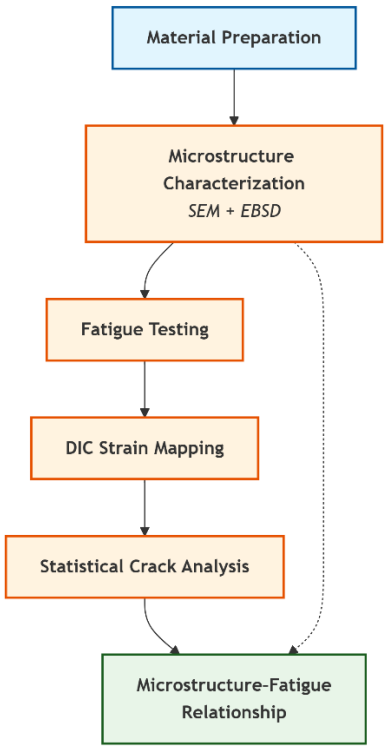

Figure 1. Experimental workflow for microstructure-controlled fatigue crack initiation and propagation in super duplex stainless steel 2507

Measurement uncertainty for a DIC system was estimated to be within ± 50 microstrain. Although optimization of speckle coating was performed for speckle pattern quality, a small change in material properties may arise due to speckle coating, which may influence crack initiation. However, it was observed that speckle coating does not significantly influence crack initiation locations when compared to SEM observations.

3. RESULTS AND DISCUSSION

3.1 Fatigue crack initiation site analysis

A comprehensive statistical investigation of fatigue crack initiation locations indicates a significant influence of their location in the material's microstructure, as demonstrated in Table 2. The most striking observation is that 78.2% of all fatigue cracks initiated at austenite-ferrite phase boundaries, thus reinforcing the significance of phase boundaries in controlling fatigue crack initiation in super duplex stainless steel 2507.

This trend significantly exceeds crack initiation at grain boundaries within individual phases, in contrast to single-phase alloys where grain boundaries usually dominate crack nucleation. The results are consistent with earlier observations in duplex stainless steels [3, 17], while the higher fraction observed here reflects the increased interface sensitivity of super duplex grades.

The high level of stress concentration factor at phase boundaries (2.8 ± 0.4) is attributed to the difference in the elastic modulus and strain incompatibility between the austenite and ferrite phases of the duplex stainless steel material, which are of different crystal structures: FCC for austenite and BCC for ferrite. The level of stress concentration at phase boundaries has been reported to be similar for duplex stainless steel by experimental and numerical studies [18, 19]. The highest stress concentration factor is at triple points with a value of 3.4 ± 0.6; however, their probability of occurrence is low.

Table 2. Statistical distribution of fatigue crack initiation sites and associated stress concentration factors

Initiation Site	Percentage (%)	Stress Concentration Factor	Cycles to Initiation ($\times 10^3$)
Phase boundary (γ/α)	78.2	2.8 ± 0.4	12.5 ± 3.2
Ferrite grain boundary	12.4	2.1 ± 0.3	18.6 ± 4.1
Austenite grain boundary	6.8	1.9 ± 0.2	21.4 ± 5.0
Triple junctions	2.1	3.4 ± 0.6	8.8 ± 2.1
Others	0.5	1.6 ± 0.2	24.0 ± 5.5

Figure 2 shows representative SEM images of fatigue crack initiation at austenite-ferrite phase boundaries and at grain boundaries of individual phases.

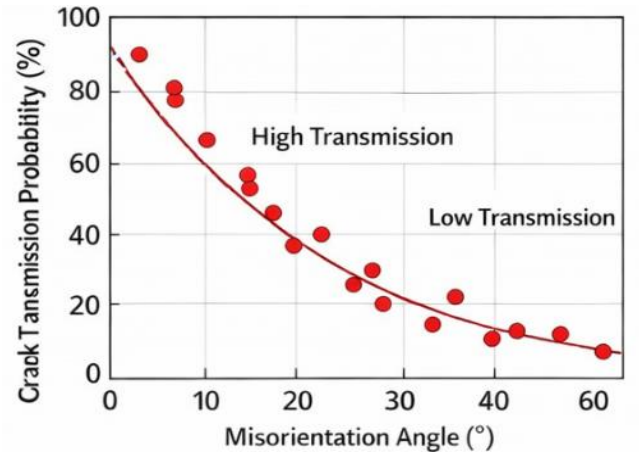

Figure 2. Scanning Electron Microscopy (SEM) images of fatigue crack initiation

3.2 Early crack propagation kinetics and phase-dependent behavior

Significant phase dependence behavior indicates a notable phase dependence, as presented in Table 3. For short crack lengths ranging from 10 to 25 μm, the crack growth rates in the austenitic phase are about 34% lower compared to those in the ferritic phase. This suggests that the austenitic phase has better resistance to early crack propagation.

The rates of crack growth measured experimentally can be related to the Paris model for crack growth due to fatigue. In accordance with the Paris relationship, increased stress intensity factors are related to increased rates of crack growth.

The lower rates of crack growth measured for the austenitic phase (Table 3) are related to a reduced stress intensity factor due to increased plastic deformation and crack blunting in the FCC structure of the austenitic phase.

Table 3. Phase-dependent early fatigue crack growth rates

Crack Length (μm)	Austenite da/dN (mm/cycle)	Ferrite da/dN (mm/cycle)	Difference (%)
10–25	$(2.1 \pm 0.4) \times 10^{-6}$	$(3.2 \pm 0.6) \times 10^{-6}$	34
50–100	$(6.5 \pm 1.1) \times 10^{-6}$	$(9.1 \pm 1.4) \times 10^{-6}$	29
100–200	$(1.1 \pm 0.2) \times 10^{-5}$	$(1.6 \pm 0.3) \times 10^{-5}$	31

These results are found to be consistent with the existing studies on duplex steels/super duplex steels [3, 20], where the improved fracture toughness and work hardening of austenite have been found to result in reduced crack growth rates. Recent high-resolution EBSD and TEM investigations have shown the improved capacity of austenite to absorb cyclic plasticity through improved dislocation activity [20, 21]. The crack growth rate along the interface is found to be intermediate due to the benefits of crack deflection and blunting [22].

3.3 Crack path characteristics and microstructural interactions

The crack path morphology varies substantially with crack propagation regions, as indicated in Table 4.

Table 4. Crack deflection, branching, and surface roughness characteristics

Crack Location	Deflection Angle (°)	Branching Frequency (/100 μm)	Surface Roughness (μm)
Austenite	15.6 ± 8.2	1.8 ± 0.9	0.85 ± 0.25
Ferrite	8.9 ± 4.1	0.9 ± 0.4	0.52 ± 0.18
Phase boundary	22.4 ± 12.5	3.4 ± 1.8	1.12 ± 0.35

Phase boundary cracks show the most complex paths, with high deflection angles and branching frequency. This behavior is attributed to crystallographic mismatch and slip incompatibility across the interface, consistent with EBSD-based fatigue studies in duplex alloys [23].

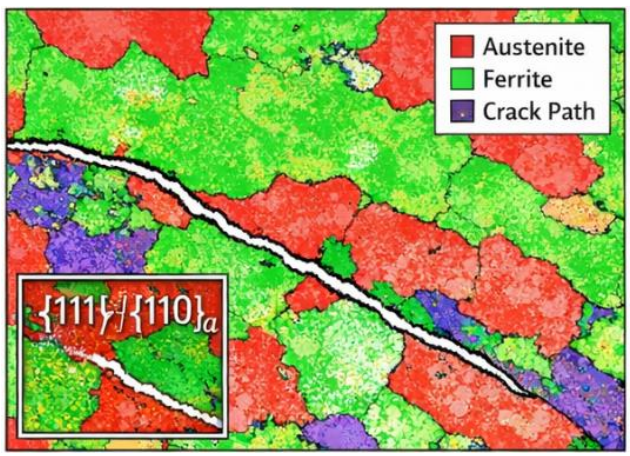

Figure 3. Electron Backscatter Diffraction (EBSD) orientation map showing crack transmission across low- and high-angle boundaries

Figure 3 presents EBSD orientation maps illustrating crack transmission and deflection across low- and high-misorientation boundaries.

3.4 Strain distribution analysis using Digital Image Correlation

Quantitative strain measurements obtained by DIC are summarized in Table 5.

Table 5. Maximum principal strain and plastic zone size measured by Digital Image Correlation (DIC)

Microstructural Feature	Max Strain ($\times 10^{-3}$)	Strain Concentration Factor	Plastic Zone Size (μm)
Triple junction	4.9 ± 1.2	2.3 ± 0.5	22.8 ± 5.2
Phase boundary	3.8 ± 0.8	1.8 ± 0.3	15.2 ± 3.5
Crack tip (10 μm ahead)	8.2 ± 1.8	3.1 ± 0.6	45.6 ± 8.9

Strain localization is observed maximally in triple junctions and phase boundaries, in direct correlation with crack initiation statistics. Recent DIC-based investigations in duplex steels have reaffirmed the importance of strain localization in fatigue damage accumulation processes [24, 25]. Figure 4 shows some representative DIC strain maps that highlight localization in phase boundaries and triple junctions.

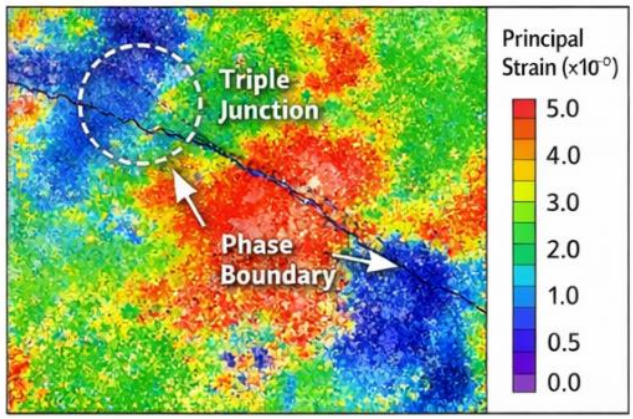

Figure 4. Digital Image Correlation (DIC) strain map showing strain localization at phase boundaries and triple junctions

The strain localization detected using DIC directly influences the stress intensity factor at the crack tip. Regions exhibiting high strain concentration correspond to higher local stress intensity factors, which promotes crack initiation and early crack growth according to the Paris law framework.

3.5 Electron Backscatter Diffraction–based crack transmission analysis

To further quantify the crystallographic influence on fatigue crack behavior, analyses using MTEX software were carried out. The Taylor factor maps obtained using MTEX software indicated that areas where the Taylor factor was high (> 3.2) experienced more localized strain and are preferred sites for fatigue crack nucleation, especially in areas around phase boundaries. Grain boundary energy calculations indicated that grain boundaries where the energy was high (> 0.8 J/m²)

experienced a lower probability in crack transmission, which was in conformity with observations from EBSD maps where crack deflection was noted. The influence of grain boundary misorientation on crack transmission probability is depicted in Table 6.

Table 6. Effect of misorientation angle on crack transmission behavior

Misorientation Range (°)	Transmission Probability (%)	Deflection Angle (°)
5–15	85.2 ± 8.5	12.3 ± 6.2
15–30	62.8 ± 12.1	28.5 ± 15.8
> 45	18.9 ± 9.8	62.8 ± 28.5

The grain boundary misorientation has a significant impact on the stress intensity factor at the crack tip. Grain boundaries that are high-angle act as barriers for crack transmission; this leads to a decrease in the value of ΔK experienced by the crack.

This explains the reduced likelihood of crack transmission for grain boundary misorientation above 45°. The study also proves that high-angle grain boundaries hinder crack transmission, which is in agreement with classical grain boundary engineering theory [26] and fatigue EBSD theory [21].

3.6 Statistical analysis of fatigue life distribution

Weibull analysis is shown in Table 7, confirming consistent fatigue response with a shape parameter of approximately 3.2.

Table 7. Weibull fatigue life parameters

Stress Level (MPa)	β	η (cycles)	N10%	N90%
300	3.3	7.2×10^6	3.9×10^6	1.1×10^7
400	3.1	4.3×10^5	2.2×10^5	6.8×10^5

The high Weibull modulus indicates reduced scatter and reliable fatigue performance, consistent with recent probabilistic fatigue studies on duplex steels [27].

3.7 Fractographic analysis and failure mechanisms

Quantitative fractographic analysis results are presented in Table 8, which shows that fatigue striations were found to be the predominant feature, occupying 68.5 ± 8.2% of the fracture surface. This confirms that the failure process is predominantly controlled by fatigue crack growth. The presence of quasi-cleavage features (18.2 ± 5.1%) indicates that there were localized brittle-like features, which can be ascribed to microstructural effects and stress concentration phenomena.

Table 8. Distribution of fracture surface features

Feature	Area Fraction (%)
Fatigue striations	68.5 ± 8.2
Quasi-cleavage	18.2 ± 5.1
Secondary cracks	3.1 ± 1.5
Ductile dimples	8.9 ± 3.2

The presence of secondary cracks (3.1 ± 1.5%) indicates that there were crack branching phenomena, which had a localized effect on the crack growth process. The presence of ductile dimples (8.9 ± 3.2%) was found to be localized to the final fracture region, which indicates that ductile overload was present after extensive fatigue damage accumulation [28], Similar fractographic features and failure mode transitions have been reported in recent SEM-based studies, highlighting the role of local stress state and material heterogeneity in governing fracture morphology [29].

The fractography presented in Figure 5 show the presence of fatigue striations and quasi-cleavage features, which confirms the fractographic analysis results. It can therefore be confirmed that the material had failed due to fatigue, as indicated by the mechanical testing results.

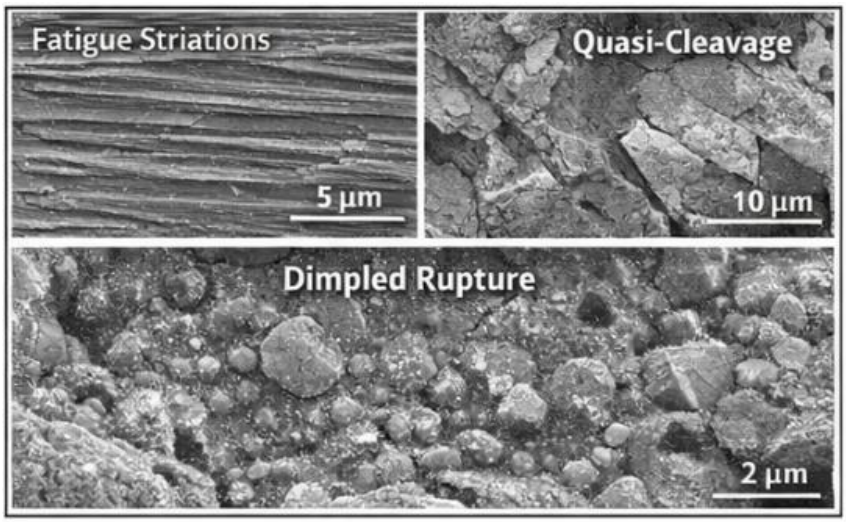

Figure 5. Scanning Electron Microscopy (SEM) fractography showing fatigue striations and quasi-cleavage features in ferrite

3.8 Microstructure-property relationships and design implications

From the results, it is evident that significant microstructure-property relationships relevant to fatigue optimization of duplex stainless steels, along with their design implications, are as follows:

- Phase Boundary Engineering: Fatigue crack initiation on the austenite-ferrite phase boundaries was determined to be predominant (78.2%, Table 2), and by

controlling the stress concentrations on the phase boundaries by thermomechanical control and composition control to limit crack transfer across the phase boundaries, particularly by generating more high-misorientation phase boundaries (Table 6).

- Phase Balance Optimization: Differences in crack growth rates between austenite and ferrite phases, with crack growth occurring approximately 34% more slowly in austenite than ferrite (Table 3), suggest optimization of the phase balance within metallurgical limits can improve the fatigue properties of duplex stainless steels. This is consistent with earlier microstructural optimization studies conducted on super duplex stainless steels [30] and is supported by strain localization data (Table 5).
- Crystallographic Texture Control: The crack transmission across the phase boundaries has a strong dependence on misorientation (Table 6, Figure 3). By controlling the texture of the duplex stainless steel, it is possible to generate stronger crack barriers, with the crack propagation direction corresponding to specific {111} planes in austenite and {110} planes in ferrite to minimize the resolved shear stresses (Table 3). In addition, regions with higher Taylor factor obtained from MTEX analysis show higher strain localization and tendency for crack initiation.
- Microstructural Scale Effects: The plastic zones are also related to the crack initiation process. A refinement in the grain size can lead to a higher crack deflection and lower stresses. Table 5 and Figure 3 show that plastic zones of 15–45 μm are desirable for fatigue resistance.
- Statistical Design Considerations: The fatigue life is Weibull distributed with shape parameter $\beta \approx 3.2$, which indicates low scatter and good predictability (Table 7). Fractography analysis shows that striation-controlled crack propagation is dominant (Table 8 and Figure 5). This is advantageous for statistically designed fatigue performance, as the microstructural parameters are well controlled.

Overall, the integration of EBSD, DIC, fractographic analysis, and statistical modeling provides a robust framework for microstructure-based fatigue design of duplex stainless steels. These findings establish actionable processing–structure–property relationships that can be directly implemented in industrial material design and optimization.

4. CONCLUSIONS

The current research offers a detailed experimental investigation of fatigue crack initiation and early-stage propagation in super duplex stainless steel 2507. Emphasis is given to microstructural and crystallographic effects. Advanced characterization methods are used to establish quantitative correlations between microstructure and fatigue properties.

In the case of fatigue crack initiation, the results show that ~78% of fatigue crack initiation takes place at the austenite-ferrite interface. Triple junctions also show high stress/strain concentration, hence high fatigue crack nucleation rates.

In terms of early-stage propagation, the results indicate that austenite consistently has lower rates of fatigue crack propagation compared to ferrite. This is because ferrite exhibits higher crack growth rates due to lower work-hardening capability compared with austenite. The propagation rates at the interface are intermediate. EBSD results on crystallographic aspects indicate that the transmission of fatigue cracks through phase boundaries depends on boundary misorientation. Low-angle boundaries allow for transmission, while high-angle boundaries impede transmission, resulting in deflection. DIC results indicate that strain localization is highest at triple junctions and phase interfaces. Fatigue life results indicate that the fatigue life follows a Weibull distribution with high shape parameters. This implies low scatter in results and high reproducibility. Fractographic analysis also provides evidence of fatigue characterization in 2507.

Quantitative correlations between microstructure and fatigue properties are established. Texture control is also shown to be effective in enhancing fatigue resistance. The paper also demonstrates the applicability of probabilistic design. The integrated experimental approach is also shown to be useful in the analysis of complex multi-phase materials.

REFERENCES

[1] Maurya, A.K., Pandey, S.M., Chhibber, R., Fydrych, D., Pandey, C. (2024). Corrosion performance of super duplex stainless steel and pipeline steel dissimilar welded joints: A comprehensive investigation for marine structures. The International Journal of Advanced Manufacturing Technology, 135: 1009-1033. https://doi.org/10.1007/s00170-024-14596-3

[2] Li, T.Q., Wang, K., Lei, Y.C. (2024). A review of welding process for UNS S32750 super duplex stainless steel. Materials, 17(21): 5215. https://doi.org/10.3390/ma17215215

[3] Prunbauer, M., Raninger, P., Ecker, W., Rester, M., Ebner, R. (2024). A comprehensive material model for the super-duplex stainless steel SAF2507 in a welding environment. Metals, 14(2): 153. https://doi.org/10.3390/met14020153

[4] Pan, Q.S., Lu, L. (2025). Fatigue in metals and alloys. Nature Materials, 25: 357-365. https://doi.org/10.1038/s41563-025-02308-5

[5] Wang, C., Zhang, W.B., Li, C., Wang, D.G., Wahab, M.A. (2023). Two-scale analysis of fretting fatigue crack initiation in heterogeneous materials using continuum damage mechanics. International Journal of Solids and Structures, 269: 112215. https://doi.org/10.1016/j.ijsolstr.2023.112215

[6] Wu, X.H., Song, Z.G., Liu, L.Z., He, J.G., Zheng, L. (2022). Effect of secondary austenite on fatigue behavior of S32750 super duplex stainless steel. Materials Letters, 322: 132487. https://doi.org/10.1016/j.matlet.2022.132487

[7] Yao, Z.H., Hao, J., Zhang, H.Z., Li, C.Y., Dai, W.B. (2024). Influence of force amplitude on microstructures evolution, fatigue behavior, and ratcheting failure mechanism of 1Cr18Ni10Ti pressure pipe. Engineering Fracture Mechanics, 298: 109923. https://doi.org/10.1016/j.engfracmech.2024.109923

[8] Long, D.J., Liu, Y., Wan, W.F., Dunne, F.P.E. (2023). A microstructure-sensitive analytical solution for short fatigue crack growth rate in metallic materials. International Journal of Mechanical Sciences, 253:

108365. https://doi.org/10.1016/j.ijmecsci.2023.108365
[9] Li, X., Liang, Q.L., Liang, C.X., Wang, D., Li, S.Z., Ding, X.D. (2026). Fatigue resistant elastocaloric effect in TiNi via texture-precipitate synergy. Nature Communications, 17: 2147. https://doi.org/10.1038/s41467-026-68835-0
[10] Shan, M., Muhammad, K.F., Muhammad, M.R., Wong, Y.H., Yoshida, M. (2025). Advancements in copper and silver sintering as interconnect materials in electronics applications: Review. Journal of Materials Science: Materials in Electronics, 36: 1803. https://doi.org/10.1007/s10854-025-15835-3
[11] Hebert, J., Khonsari, M. (2022). The application of digital image correlation (DIC) in fatigue experimentation: A review. Fatigue & Fracture of Engineering Materials & Structures, 46(4): 1256-1299. https://doi.org/10.1111/ffe.13931
[12] Chen, M., He, J.S., Wang, M.M., Li, J.S., Xing, S.L., Gui, K.X., Wang, G., Liu, Q. (2022). Effects of deep cold rolling on the evolution of microstructure, microtexture, and mechanical properties of 2507 duplex stainless steel. Materials Science and Engineering: A, 845: 143224. https://doi.org/10.1016/j.msea.2022.143224
[13] Bogusz, P., Krasoń, W., Pazur, K. (2024). Application of digital image correlation for strain mapping of structural elements and materials. Materials, 17(11): 2577. https://doi.org/10.3390/ma17112577
[14] Yang, R., Li, Y., Zeng, D., Guo, P. (2022). Deep DIC: Deep learning-based digital image correlation for end-to-end displacement and strain measurement. Journal of Materials Processing Technology, 302: 117474. https://doi.org/10.1016/j.jmatprotec.2021.117474
[15] ASTM E562-19. (2020). Standard test method for determining volume fraction by systematic manual point count. https://doi.org/10.1520/E0562-19
[16] Prior, D.J., Boyle, A.P., Brenker, F., Cheadle, M.C., et al. (1999). The application of electron backscatter diffraction and orientation contrast imaging in the SEM to textural problems in rocks. American Mineralogist, 84(11-12): 1741-1759. https://doi.org/10.2138/am-1999-11-1204
[17] Liu, L.X., Wu, Q.F., Zhu, J.X., Bai, X.Y., Jia, Y.H., He, F., Li, J.J., Wang, J.C., Wang, Z.J. (2025). Revealing cracking behavior of phase and grain boundaries in dual-phase high-entropy alloy at elevated temperatures. Materials Characterization, 220: 114703. https://doi.org/10.1016/j.matchar.2024.114703
[18] Wang, W.X., Wang, J.J., Wang, Q., Huang, X.T., Lu, G., Liu, Y.J., Liu, C.M. (2023). Ferrite-austenite synergistic deformation behavior in a 2205 duplex stainless steel containing equiaxed austenite domains. Materials Characterization, 205: 113363. https://doi.org/10.1016/j.matchar.2023.113363
[19] Gargalis, L., Karavias, L., Graff, J.S., Diplas, S., Koumoulos, E.P., Karaxi, E.K. (2023). A comparative investigation of duplex and super duplex stainless steels processed through laser powder bed fusion. Metals, 13(11): 1897. https://doi.org/10.3390/met13111897
[20] Gao, F., Gao, Z.L., Zhu, Q.Y., Yu, F.X., Liu, Z.Y. (2022). Deformation behavior of retained austenite and its effect on plasticity based on in-situ EBSD analysis for transformable ferritic stainless steel. Journal of Materials Research and Technology, 20: 1976-1992. https://doi.org/10.1016/j.jmrt.2022.07.160
[21] Bao, S., Feng, H., Song, Z.G., He, J.G., Wu, X.H., Gu, Y. (2025). Deformation behavior of S32750 duplex stainless steel based on in situ EBSD technology. Materials, 18(9): 2030. https://doi.org/10.3390/ma18092030
[22] Zhang, Y., Wang, S.Y., Xu, G.T., Wang, G., Zhao, M.H. (2022). Effect of microstructure on fatigue-crack propagation of 18CrNiMo7-6 high-strength steel. International Journal of Fatigue, 163: 107027. https://doi.org/10.1016/j.ijfatigue.2022.107027
[23] Dong, Z.L., Xie, X.F., Li, J.W., Wan, Y., Wang, C.L. (2023). Microstructure formation and fatigue performance of duplex stainless steel 2205 welded joints by electric resistance welding. Archives of Civil and Mechanical Engineering, 23: 180. https://doi.org/10.1007/s43452-023-00726-3
[24] Basu, S., Jaya, B.N., Seekala, H., Phani, P.S., Patra, A., Ganguly, S., Dutta, M., Samajdar, I. (2023). Correlative characterization and plasticity modeling of microscopic strain localizations in a dual phase steel. Materials Characterization, 197: 112704. https://doi.org/10.1016/j.matchar.2023.112704
[25] Sriba, A., Bouquerel, J., Vogt, J.B. (2022). DIC-aided analysis of the fatigue behaviour of a welded 316L stainless steel. Welding in the World, 66: 1915-1927. https://doi.org/10.1007/s40194-022-01355-9
[26] Rawat, N.K., Mishra, A.K., Jain, N., Ogata, S., Verma, A. (2026). A comprehensive review on the formation and evolution of faceted grain boundaries with their implications on material properties. Metals and Materials International, 32: 18-49. https://doi.org/10.1007/s12540-025-02031-5
[27] Moreira, A.B., Costa, A.P.O., Ribeiro, L.M.M., Santos, A.D., de Jesus, A. (2024). On the correlation between fatigue behaviour and the multiphase microstructure of a super duplex stainless steel. Engineering Fracture Mechanics, 307: 110341. https://doi.org/10.1016/j.engfracmech.2024.110341
[28] Geng, X., Qin, D., Ping, Y., Deng, J.L. (2022). Effect of overload on low cycle fatigue crack growth behavior considering accumulative plastic damage. Journal of Failure Analysis and Prevention, 22: 346-355. https://doi.org/10.1007/s11668-021-01306-4
[29] Faisal, B.M., Abed, K.A., Mohammed, A.A., Hussein, E.K., Sharaf, H.K., Santos, T., Santos, C. (2024). Investigation of the high velocity impact test on the curved glass fiber reinforced plastic (GFRP) composites using explicit dynamics analysis. International Journal on Advanced Science, Engineering and Information Technology, 14(6): 2084-2089. https://doi.org/10.18517/ijaseit.14.6.10417
[30] Ballésio, S., Le Hong, T., Dhondt, M., Doudard, C., Szmytka, F. (2024). Manufacturing of 2507 super duplex stainless steel by laser powder-directed energy deposition: Process optimization and microstructure analyses. International Journal of Advanced Manufacturing Technology, 132: 5663-5682. https://doi.org/10.1007/s00170-024-13673-x

NOMENCLATURE

a	crack length
da/dN	fatigue crack growth rate

C	paris law material constant
m	paris law exponent
ΔK	stress intensity factor range
Kt	stress concentration factor
σ	applied stress amplitude
R	stress ratio (σ_min/σ_max)
N	number of loading cycles
Nf	number of cycles to failure
β	weibull shape parameter
η	weibull scale parameter

Greek symbols

ε	local strain
α	phase fraction parameter
β	weibull distribution shape parameter
θ	grain boundary misorientation angle
μ	friction or slip coefficient

Subscripts

γ	austenite phase
α	ferrite phase
tip	crack tip
max	maximum value
min	minimum value